Full Paper
doi.org/10.1002/chem.202003259

Inter/Intramolecular Interactions

Inter- and Intramolecular Aryl–Aryl Interactions in Partially Fluorinated Ethylenedioxy-bridged Bisarenes**

Jan-Henrik Weddeling, Yury V. Vishnevskiy,* Beate Neumann, Hans-Georg Stammler, and Norbert W. Mitzel*[a]

Abstract: Several ethylenedioxy-bridged bisarenes with a variety of type and number of aryl groups were synthesized to study non-covalent dispersion-driven inter- and intramolecular aryl–aryl interactions in the solid state and gas phase. Intramolecular interactions are preferably found in the gas phase. DFT calculations with and without dispersion correction show larger interacting aromatic groups increase the stabilization energy of folded conformers and decrease the intermolecular centroid–centroid distance. Single-molecule structures generally adopt folded conformations with short intramolecular aryl–aryl contacts. Gas electron diffraction experiments were performed exemplarily for 1-(pentafluorophenoxy)-2-(phenoxy)ethane. A new procedure for structure refinement was developed to deal with the conformational complexity of such molecules. The results are an experimental confirmation of the existence of folded conformations of this molecule with short intramolecular aryl–aryl distances in the gas phase. Solid-state structures are dominated by stretched structures without intramolecular aryl–aryl interactions but interactions with neighboring molecules.

Introduction

Intra- or intermolecular interactions between aromatic systems are of importance for different categories in molecular science. Supramolecular recognition processes,[1] interplay of DNA side-chains,[2] or host–guest complexation[3] as well as crystal engineering[4] are some prominent examples. Many experimental and theoretical studies deal with such interactions, however, they are still far from being completely understood. The simplest model for aryl–aryl interactions is the benzene dimer.[5] In the solid state, the benzene rings arrange in T-shaped or herringbone structures, described as σ–π interactions;[6] a parallel arrangement of the rings is not favored. In contrast to the arrangement in the solid state, the results of gas-phase and theoretical studies show the parallel displaced or offset as well as the rare sandwich structures to be more important under these conditions.[7] Easier to predict are the interactions between benzene (C_6H_6) and its perfluorinated analog hexafluoro-benzene (HFB, C_6F_6). Both pure substances arrange in herringbone-like structures in the solid state,[8] but the equimolar mixture of benzene and HFB crystallizes in a parallel displaced structure of alternating HFB and benzene units. Strong intermolecular C_6H_6···C_6F_6 stacking interactions increase the melting point by about 18 °C relative to the individual solid substances.[9,10] This phenomenon was discovered by Patrick and Prosser[10] and was first interpreted by an interaction of opposing quadrupole moments of both substances (C_6H_6: −6.69, C_6F_6: 7.89 a.u.).[9] Later studies pointed out that London dispersion (LD) forces, the attractive part of van der Waals interactions,[11] have a significant impact on the total interaction energy.[12] To analyze this phenomenon, different aromatic groups were linked with rigid or flexible backbones and investigated in different phases and by different methods.[13]

Recently, our group studied stacking interactions between different types of halogenated and non-halogenated phenyl groups linked by different backbones in various phases. Compounds with phenyl and perfluorophenyl rings bridged by (sila)propyl chains receive stabilization by intermolecular aryl–aryl stacking interactions in the solid state,[14] whereas free molecules, studied by gas electron diffraction (GED), find their energetic minima as conformers bearing intramolecular aryl–aryl interactions. 1,1,2,2-Tetramethyldisilanes, substituted with symmetric or asymmetric pairs of phenyl and/or perhalogenated (F, Cl) phenyl groups also show strong π-interactions.[15,16] The aggregation in solid state was found to be significantly stabilized by intramolecular aryl–aryl interactions. Gas electron diffraction and SAPT (symmetry-adapted perturbation theory) cal-

[a] J.-H. Weddeling, Dr. Y. V. Vishnevskiy, B. Neumann, Dr. H.-G. Stammler, Prof. Dr. N. W. Mitzel
Lehrstuhl für Anorganische Chemie und Strukturchemie
Fakultät für Chemie, Universität Bielefeld
Universitätsstraße 25, 33615 Bielefeld (Germany)
E-mail: yury.vishnevskiy@uni-bielefeld.de
mitzel@uni-bielefeld.de

[**] A previous version of this manuscript has been deposited on a preprint server (https://doi.org/10.26434/chemrxiv.12643154.v1).

Supporting information and the ORCID identification number(s) for the author(s) of this article can be found under: https://doi.org/10.1002/chem.202003259.

culations demonstrate the untypical *syn*-conformers to be stabilized by large dispersion contributions.

From our experience with bridged bisarenes, we learned that the type of interaction partners and the linking backbone is important for the stabilization of gas-phase and solid-state structures. We were interested if more flexibility and a modified electronic surrounding, by heteroatoms in the bridge, would influence such interactions. Therefore, we report here investigations employing a new four-atomic ethylenedioxy linker unit (-OCH_2CH_2O-) between a variety of interacting aromatic systems.

Results and Discussion

Before we started synthesizing such model systems, we performed preliminary calculations to evaluate whether intramolecular aryl–aryl interactions are also possible with the ethylenedioxy linker unit. At first, we investigated the electronic and mesomeric effect of the new linker and whether the oxygen atoms have an influence on the conformations or electron density of the interacting aromatic systems. As the simplest model system for our linker unit, we performed a potential energy scan (PBE0-D3/def2-TZVP) around the C–C-bond of H_3C-OCH_2CH_2O-CH_3 (Figure S38 in the Supporting Information). We found two minima, *gauche* and *anti*, of nearly the same energy. Therefore, we can assume that the relative positions of the oxygen atoms to each another in the -OCH_2CH_2O- unit do not significantly influence the conformational energies.

The electronic effects of the oxygen substituents on the aryl groups were analyzed by inspection of the electrostatic potential (ESP) surface of compound **2** in its stretched form. As shown in Figure 1, the effect of the oxygen atoms on the electron density of both aromatic rings is not very pronounced, in terms of a distortion of the ESP. As mentioned for aromatic systems investigated before,[17] the electrostatic potential values on the surface of the phenyl group are negative (blue) whereas the surface of the perfluorophenyl group has a positive ESP (yellow/red). The complementary polarization of the aryl groups should lead to attractive interactions between these functions. These interactions would necessarily be intramolecular for isolated molecules in the gas phase, but difficult to predict for the solid state, where alternative intermolecular interactions are possible.

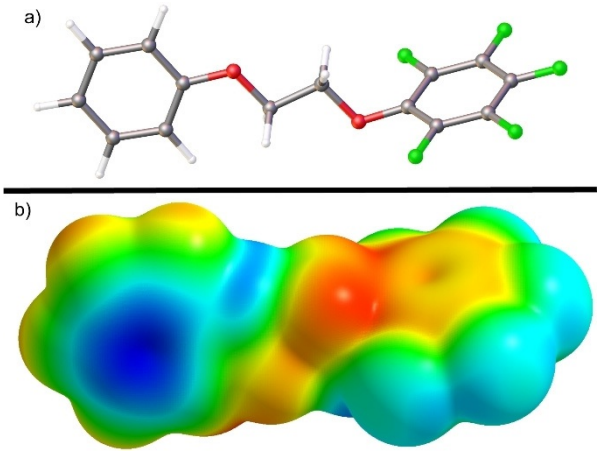

Figure 1. Stretched conformation of **2** (a) and its total electrostatic potential (ESP) (b) mapped onto the isosurface (0.0005 a.u.) of the electron density by using AIMAll[18] at the PBE0-D3/def2-TZVP level of theory. Blue and red areas correspond to the negative and positive ESP values with maximal magnitudes, respectively.

To see whether folded conformers with intramolecular stacking interactions represent the favored conformation in the gas phase, we used the CREST procedure[19] for a global search of stable conformers at the GFN2-xTB[20] level of theory for compounds **2**–**10**. We additionally inspected compound **1**, the analog of **2**, C_6H_5-$(CH_2)_4$-C_6F_5, with an oxygen-free four-atomic bridge, to prove that the predicted conformers are largely independent of the preferred stereochemical effects of the ethylenedioxy linker.

With a series of calculations on compounds **1**–**10** (Scheme 1), we decided if the examined compound was worthy of being synthesized and analyzed experimentally. For one example, compound **2**, we determined the structure of a free molecule in the gas phase by means of gas electron diffraction (GED). This investigation was supported by a more detailed description with computational methods. This will be described below and is outlined in detail in the Supporting Information.

The minima found for compounds **1**–**10** at the global search were structure-optimized at the PBE0/def2-TZVP level of theory by using Gaussian 16[22] and are listed in the Supporting Information. The calculations were performed with and with-

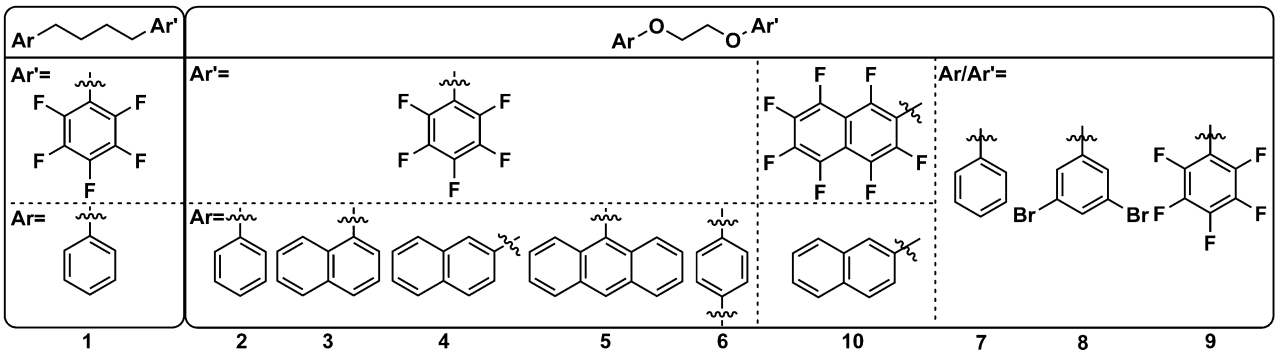

Scheme 1. Model compounds **1**–**10**.

out D3 correction for dispersion interactions[21] to analyze if the intramolecular aryl–aryl interactions for folded conformers are caused solely by electrostatic effects. Along with the expected folded and stretched structures, we also found minima with half-folded structures (e.g., compound **2**; see Figure 2).

For these conformers, the aromatic ring systems are not in a parallel offset orientation relative to one another; instead, they are twisted or adopt T-shaped arrangements of their aryl rings (similar to the arrangements in the crystal structures of pure benzene or hexafluorobenzene). They also have generally longer centroid–centroid distances (see the Supporting Information). These half-folded structures represent in many cases the global minima if no D3 dispersion correction was applied. For calculations with D3 dispersion correction, folded and half-folded conformers have similar energies. The stretched conformers were modelled by optimizing the structures found in the solid state (see below). In general, the application of D3 corrections for dispersion leads to significantly lower energies of (half-)folded conformers, with small centroid–centroid distances. For all compounds with at least one pentafluorophenyl group, the folded structures are more favorable than the stretched ones by $\Delta E = 2$–24 kJ mol^{-1} (Table 1).

The centroid–centroid distances are comparable to those in bisarene compounds, which our group investigated earlier in the solid state (XRD) and by gas electron diffraction (e.g., shortest centroid distances: $PhCH_2CH_2CH_2Ph_f$: 3.50(2) Å; $PhSiMe_2SiMe_2Ph_f$: 3.76(3) Å).[14,22] The enlargement of the non-fluorinated (**2**, **3**, **5**) or fluorinated (**4**, **10**) ring system influences the strength of the interactions and can be seen by comparing the decreasing centroid–centroid distances (Figure 3). Owing to the greatest interacting surfaces, we found the largest stabilization energies for compound **10**. The ethylenedioxy-bridge generally allows close intramolecular aryl–aryl contacts and there is a clear relationship between the size of the aromatic systems and the centroid–centroid distances. Furthermore, the introduction of a second $CH_2CH_2OPh_f$ unit (**2**, **6**) does lead to significantly shorter aryl–aryl contacts.

Table 1. Relative energy differences between stretched and folded conformers of compounds **1**–**10**. The relative energies of the minima E are given in kJ mol^{-1}. For $\Delta E > 0$, the folded conformer is more stable; for $\Delta E < 0$, the stretched conformer is more stable.

	$\Delta E = E_s - E_f$[a]									
method	**1**	**2**	**3**	**4**	**5**	**6**	**7**	**8**	**9**	**10**
[PBE0]	−0.3	1.1	−4.9	0.8	−16.5	3.2	−14.7	−13.2	−6.5	87.5
[PBE0-D3]	9.5	8.8	16.0	8.8	9.3	18.0	−5.6	3.1	2.1	24.0

[a] f: folded; s: stretched.

Comparison of compound **2** with its oxygen-free analog **1** again shows that the oxygen atoms in the linker unit do not influence the conformational preference significantly (Table 1). The relative energy differences of the calculations for **1** and **2**—with and without D3 correction—have the same tendency and range.

Considering the relative energy differences with and without D3 dispersion correction for each compound, **1**–**10** (Table 1), electrostatic interactions alone cannot explain the effect of stabilization of the folded conformers. If that were the case, folded conformers of compounds **3** and **5**, calculated without D3 correction, would be more stable than the stretched ones. Only by taking into account electrostatic and dispersion forces, can the stabilization of the folded conformers of partially fluorinated bisarenes be explained properly.

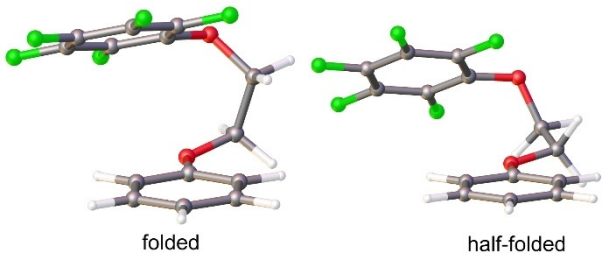

Figure 2. Calculated folded and half-folded structures of **2**.

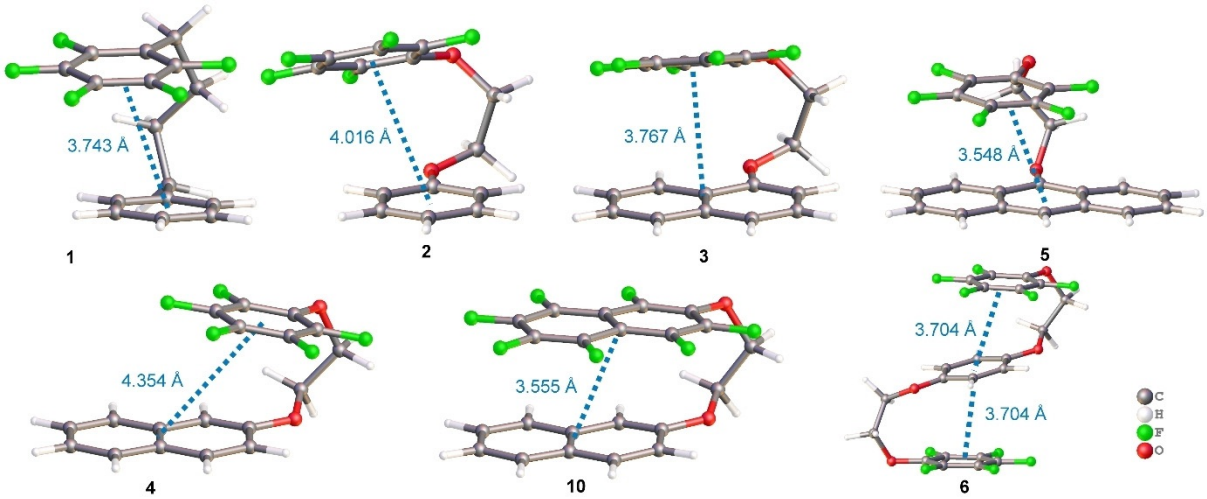

Figure 3. Minima for folded conformers of **1**–**6** and **10** calculated at the PBE0-D3/def2-TZVP level.

To explore cases without important stabilizing electrostatic components, which are dominated by dispersion effects, we investigated bisarenes with two identical aromatic substituents. Owing to the same electrostatic potential, both aryl groups should repel each other, however, surprisingly, the optimized minima for the symmetric bisarenes **8** and **9** also reveal folded structures (Figure 4).

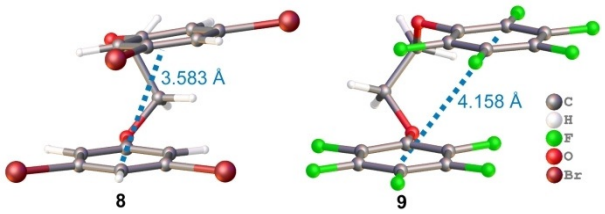

Figure 4. Folded minima of **8** (left) and **9** (right).

On first sight, this parallel displaced arrangement of the aromatic groups seems to be disfavored because of the steric hindrance of the halogen substituents and the electrostatic repulsion through of the aromatic rings—although the centroid–centroid distances are quite short. Such eclipsed conformations were also found for the perhalogenated disilanes $Ph_xSiMe_2SiMe_2Ph_x$ and are stabilized by London dispersion interactions.[15] Symmetric bisarenes without halogen substitution do not preferably arrange in folded sandwich structures. This is also the case for compound **7**.

The minimum for **7** was found for a stretched structure (Figure 5). In the latter, the inclusion of dispersion correction lowers the relative energy of the folded conformation but the repulsion between the phenyl groups still plays the dominant role. A similar free-molecule structure for the same compound was already found by calculations and fluorescence dip infrared spectroscopy (FDIR) by Buchanan et al.[24]

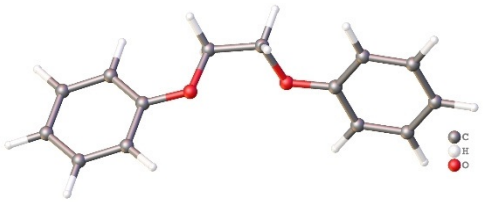

Figure 5. Calculated minimum structure for **7**.

Synthesis

For a preparative access to the model compounds, we used a modified protocol by Guo et al.[25] Scheme 2 displays an exemplary route to the asymmetric compound 1-(pentafluorophenoxy)-2-(phenoxy)ethane (**2**).

Starting from pentafluorophenol, dibromoethane, and potassium carbonate, we generated 2-(pentafluorophenoxy)ethyl bromide (**2a**). Based on this building block, we could introduce a second aryloxy group under the same conditions. This procedure allowed generation of various asymmetric bisarenes (**2**–**4**, **6**). The syntheses of symmetric bisarenes (**7**–**9**) required extended reaction times for the first etherification step. To obtain compound **5**, we generated 2-(9-anthroxy)ethyl bromide (**5a**) from anthrone and 2-bromoethanole. Compound **5a** and pentafluorophenol were then converted into **5**. Detailed information is provided in the Supporting Information. Purification by column chromatography, sublimation, and crystallization afforded the bisarenes in moderate to good yields. Compound **10** could not be synthesized yet. The compounds were characterized by NMR spectroscopy, high-resolution mass spectrometry, CHN analysis, and single-crystal X-ray diffraction.

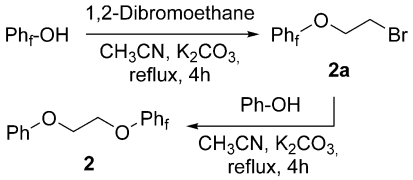

Scheme 2. Synthesis of **2** starting from pentafluorophenol.[25]

Structures in the solid state

Single crystals, suitable for X-ray diffraction, were obtained by slow evaporation of *n*-hexane solutions. Some selected structural parameters characterizing the stacking interactions are listed in Table 2. For ring systems bigger than phenyl, the centroid was defined as the centroid of all condensed six-membered rings. An aryl–aryl interaction was defined by centroid–centroid distances smaller than 4 Å.

Compounds **2**–**9** show no intramolecular aryl–aryl interactions in their solid-state structures. All molecules crystallize in stretched conformations. The arrangement of molecules in the crystal lattice follow different motifs. Compound **2** (Figure 6) forms dimeric structures whereas the phenyl and perfluorophenyl arrange in a head–tail orientation to their neighboring counterparts and undergo aryl–aryl interactions with short centroid distances [3.688(1) Å]. A second aryl–aryl interaction was found between two perfluorophenyl groups of neighboring dimers, with a distance of 3.944(1) Å, leading to an 1D polymer along the *a*-axis.

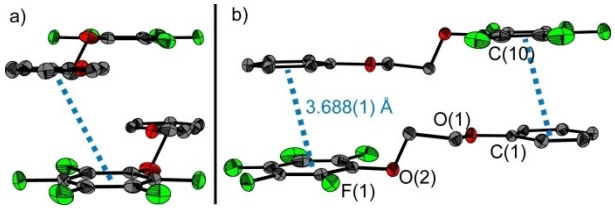

Figure 6. Molecular structure and primary aggregation of **2** in the crystalline state. (a) Side view of aggregation in the crystal lattice. (b) Interaction to neighboring molecules with an intermolecular centroid–centroid distance of 3.668(1) Å. Displacement ellipsoids are drawn at the 50% probability level. Hydrogen atoms are omitted for clarity. Symmetry operations for generating equivalent positions: 1−*x*, 1−*y*, 1−*z*.

Table 2. Selected structural parameters from solid-state structures of **2**–**9**.

	2	3	4	5	6	7	8	9
Space group	$P2_1/c$	$P2_1/c$	$P2_1/n$	$P\bar{1}$	$P2_1/c$	$P\bar{1}$	$P2_1/c$	$P\bar{1}$
R [%]	3.18	4.85	4.03	3.69	4.47	5.55	2.00	2.74
$d_{C\text{-}C}$ [Å]	3.348(2) (C1···C14)	3.338(3) (C2–C11) (C6–C9)	3.403(2) (C3–C18)	3.288(2) (C1···C19)	3.278(3) (C3···C6)	3.580(3) (C5···C9)	3.585(3) C5···C4	3.327(2) (C13···C9)
$d_{centr\text{–}centr}$ [Å]	3.688(1) 3.944(1)	3.462(1) 3.550(1)	5.026(1) 5.247(1))	3.660(1) 3.721(1)	4.431(1) 4.431(1)	5.423(1)	3.971(1)	3.553(1) 3.729(1)
$d_{plane\text{-}shift}$[Å]	1.554(2)	0.430(3) 0.418(3)	–	1.544(2) 1.371(2)	3.004(3) 2.439(4)		1.739(3)	1.376(2)
Intermolecular aryl–aryl interaction	Ph/Ph_f	$Naph/Ph_f$	–	$Anthr/Ph_f$	Ph/Ph; Ph_f/Ph_f	Ph/Ph	$Ph_{o\text{-}Br}/Ph_{o\text{-}Br}$	Ph_f/Ph_f
Aggregation motif	polymeric	columnar	–	columnar	–	–	columnar	chain-like

Unlike **2**, the crystal structure of **3** (Figure 7)contains columnar alternating stacks of perfluorophenyl and naphthyl groups from reversely oriented alternating molecules. The ring systems arrange almost perfectly above the centroid of the ring system of the neighboring counterpart. Such sandwich orientation is rarely observed.[26] Within one column, the centroid–centroid distances alternate with 3.462(1) (**A**) and 3.550(1) Å (**B**; Figure 7). **A** is the shortest intermolecular aryl–aryl distance for partially fluorinated flexibly bridged bisarenes found so far for sandwich structures in the solid state [for example, shortest centroid–centroid distances: $F_5C_6(CH_2)_2SiMe_2C_6H_5$: 3.535(1) Å; $F_5C_6(SiMe_2)_2C_6H_5$: 4.425(1) Å][14–15] and is even shorter than in the C_6F_6/C_6H_6 co-crystal (3.77 Å).[16]

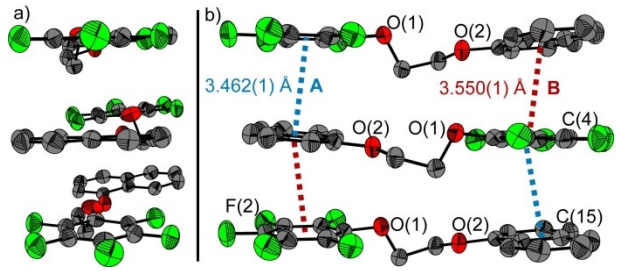

Figure 7. Molecular structure and aggregation of **3** in the crystalline state. (a) Side view of aggregation in the crystal lattice. (b) Interaction to neighboring molecules with an intermolecular centroid–centroid distance of **A** 3.462(1)/**B** 3.550(1) Å. Displacement ellipsoids are drawn at the 50% probability level. Hydrogen atoms are omitted for clarity. Symmetry operation for generating equivalent positions: $1-x$, $^1/_2+y$, $^1/_2-z$.

The variation from phenyl to naphthyl group enables each group to form two aryl contacts in the solid state. A change in substitution position—1-naphthyl (**3**) to 2-naphthyl(**4**)—to the constitution isomer **4** leads to an unexpected packing behavior. Compound **4** shows no preference for an arrangement in alternating columnar structures. Instead, we found multiple intermolecular aryl contacts (Ph_f/Ph_f, Naph/Naph, $Naph/Ph_f$) with long ranges (>5 Å; see the Supporting Information). There is no recognizable impact of π–π interactions for the arrangement in the crystal lattice.

Compound **5** (Figure 8) crystallizes in an alternating columnar structure with slightly longer intermolecular centroid distances (3.660(1) Å and 3.721(1) Å) than for **3**. This offset or parallel displaced orientation is commonly observed for aryl–aryl interactions. The angle between the plane normal and the vector between the ring centroids is about 20°.

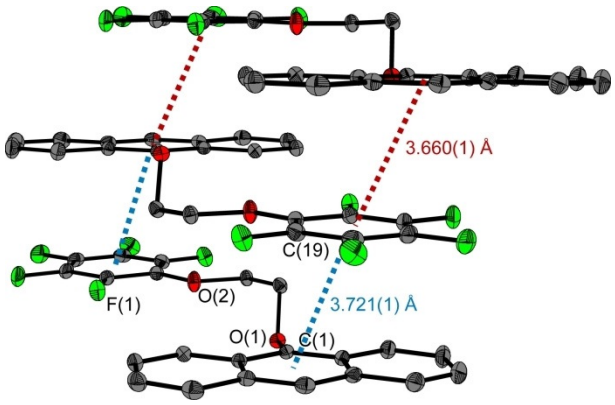

Figure 8. Molecular structure and aggregation of **5** in the crystalline state with intermolecular centroid–centroid distances of 3.660(1) and 3.721(1) Å. Displacement ellipsoids are drawn at the 50% probability level. Hydrogen atoms are omitted for clarity. Symmetry operation for generating equivalent positions: $1-x$, $1-y$, $1-z$.

To study the influence of a second $-OCH_2CH_2Ph_f$ group, trisarene **6** was synthesized. Because the molecule has twice as many fluorinated than non-fluorinated aryl rings, it is not possible to arrange in a 1:1 alternating structure as was observed for **3** or **5**, and consequently we expected a mixture of inter- and intramolecular aryl interactions.

The offset structure of **6** (Figure 9) seems to be disfavored because of the repelling surfaces of the aromatic systems and the aryl–aryl distance of 4.311(1) Å is too long for an aryl–aryl interaction. The fact that benzene and HFB, as pure substances, both prefer T-shaped arrangements in their solid-state structures, makes this structure even more interesting. Owing to the symmetry, the Ph_f groups are co-planar and the central phenyl unit is twisted by 64.1(1)° relative to them.

To analyze if the phenomenon of aryl–aryl interactions is limited to partially fluorinated bisarenes, we also investigated symmetric bisarenes with phenyl, perfluorophenyl, and 1,2-dibromophenyl groups. The solid-state structures of these compounds do not feature typical intramolecular interactions.

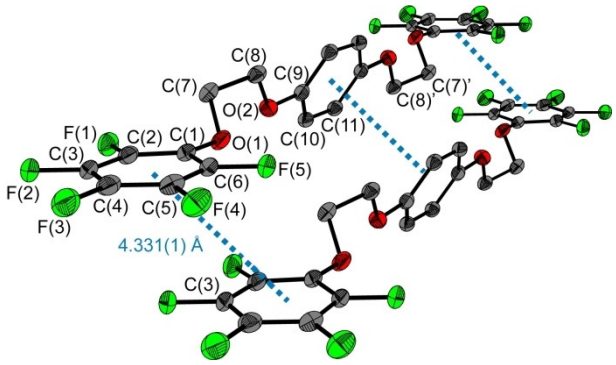

Figure 9. Molecular structure and aggregation of **6** in the crystalline state with an intermolecular centroid–centroid distance of 4.311(1) Å. Displacement ellipsoids are drawn at the 50% probability level. Hydrogen atoms are omitted for clarity. Symmetry operation for generating the second part of the molecule (1−*x*, 2−*y*, 2−*z*) and equivalent positions: +*x*, −1+*y*, +*z*.

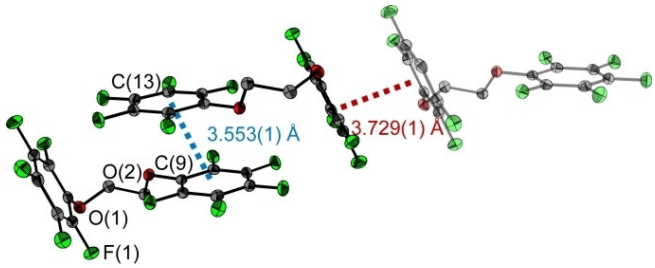

Figure 11. Molecular structure and aggregation of **9** in the crystalline state with intermolecular centroid–centroid distances of 3.553(1) Å and 3.729(1) Å. Displacement ellipsoids are drawn at the 50% probability level. Symmetry operation for generating equivalent positions: 1−*x*, 1−*y*, 1−*z*.

Whereas compound **7** shows no stacking interactions in the solid-state structures, compound **8** crystallizes in a columnar structure with a centroid–centroid distance slightly below the 4 Å limit [3.971(1) Å] (Figure 10).

Because of the long centroid distances to neighboring molecules, the interaction between two phenyl groups seems to be disfavored. The phenyl groups within one molecule of **7** are twisted against each other by 63.1°. Substitution with bromine in the *ortho*-position (**8**) leads to co-planarity of the aromatic rings within the column and a short centroid–centroid distance to neighboring molecules. This phenomenon was recently discovered in our group by investigating inter- or intramolecular π-stacking for perhalogenated groups in symmetric disilanes ($Ph_XSiMe_2SiMe_2Ph_X$; X = H, Cl, F); we recognized that π-stacking was limited to halogenated aryl groups and was not observed for hydrocarbons.[23] Such stacking interactions are stabilized primarily by London dispersion forces.

The perfluorinated compound **9** aggregates differently (Figure 11). The primary aggregation motif is a dimeric structure, with a short "inner" centroid–centroid distance of 3.553(1) Å. The "outer" Ph_f groups interact with the corresponding counterparts of neighboring dimers. This leads to endless chains running along the 111 in the crystal lattice with alternating shorter and longer aryl–aryl interactions.

To find out if we can intentionally generate the different aggregation motifs, that is, control the crystallization to some extent, we attempted to co-crystallize compounds **2**–**9** with different aromatic compounds (HFB, benzene, octafluoronaphthalene) from *n*-hexane solutions. We generated a 1:2 co-crystal of **7** and octafluoronaphthalene (OFN). It has a columnar structure of alternating entities, either one molecule of **7** or a pair of OFN molecules. Each phenyl group of **7** interacts with two neighboring OFN units (Figure 12b). The shorter contact of 3.548(1) Å is to the OFN molecule within the same unit cell, the slightly longer [3.807(1) Å] contact is to an OFN molecule of a neighboring unit cell. This packing leads to columnar structures, similar to the benzene/HFB co-crystal. The neighboring column is displaced by a half of a repetitive unit, thus the structure is additionally stabilized by inter-columnar H···F contacts [e.g., 2.48(2) Å H(6)···F(4)]. Within one sheet (along the *c*-axis), the aromatic groups are co-planar, between two sheets twisted by 6.2(1) and 3.6(1)°. Other attempts of co-crystallization could not be analyzed yet, because of the insufficient quality of the resulting crystals.

In contrast to the calculated gas-phase structures, most of the molecular structures of these compounds are found to adopt stretched conformations in the solid state. Clearly, in this phase, the number of stabilizing inter- and intramolecular interactions is larger for the stretched than for the folded conformer. As a simplest approximation of intermolecular interactions, for compound **2**, we have optimized a system of two stacked molecules in stretched conformations (Figure 13).

For this, we used the Cartesian coordinates of the dimer (A) in the crystal structure of **2**, optimized its structure, and calculated its minimum energy at the PBE0-D3/def2-TZVP level of theory. The energy of this dimeric system (A) was 54 kJ mol^{-1} (BSSE corrected) lower than twice the energy of the best folded conformation in the gas phase (B). Thus, the energetic stabilization owing to intermolecular interactions between stretched conformers is more preferable than intramolecular stabilization in the folded conformation.

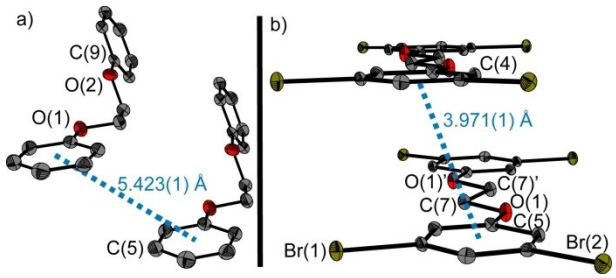

Figure 10. Molecular structures and aggregations of **7** (a) and **8** (b) in the crystalline state. Displacement ellipsoids are drawn at the 50% probability level. Hydrogen atoms are omitted for clarity. (a) Intermolecular centroid–centroid distance: 5.423(1) Å; symmetry operation for generating equivalent positions: −1+*x*, +*y*, +*z*. (b) Intermolecular centroid–centroid distance: 3.971(1) Å; symmetry operation for generating the second part of the molecule (1−*x*, −*y*, −*z*) and equivalent positions (1+*x*, +*y*, +*z*).

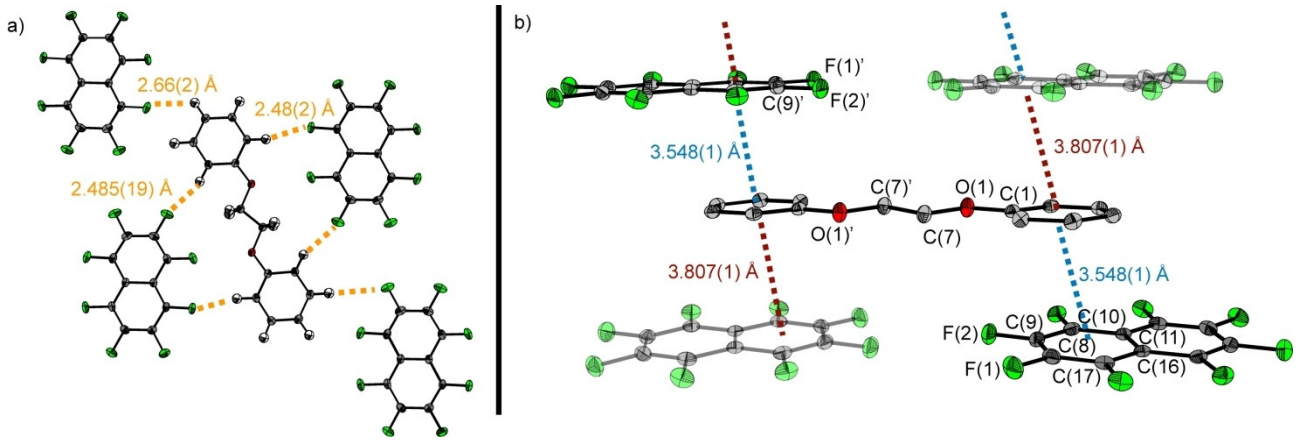

Figure 12. (a) Molecular structure and aggregation of a 1:2 co-crystal of **7** and octafluoronaphthalene in the crystalline state. Displacement ellipsoids are drawn at the 50% probability level. (a) Top view with intercolumnar H···F contacts. (b) Hydrogen atoms are omitted for clarity. Interaction in the unit cell with intermolecular centroid–centroid distances of 3.548(1) and 3.807(1) Å. The neighboring unit cells are drawn at 50% transparency level. Symmetry operation for generating the second half of the co-crystal ($-x$, $2-y$, $-z$) and equivalent positions: $+x$, $-1+y$, $+z$.

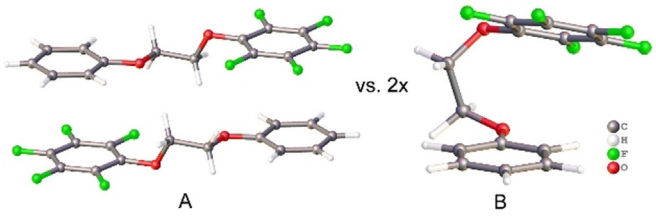

Figure 13. Comparison of inter- and intramolecular stabilization of gas-phase (B) and solid-state structures (A) of **2** at the PBE0-D3/def2-TZVP level of theory.

Structure of 2 determined by gas electron diffraction

Gas-phase structures, that is, the structures of free molecules undistorted by intermolecular interactions, can be determined by means of gas electron diffraction (GED). Owing to the very high effort to be spent, we chose **2** as a model compound for the partially fluorinated ethylenedioxy-bridged bisarenes to be studied exemplarily in the context of this present study. The structure of **2** is suitable for comparison with those of other flexibly bridged bisarenes, we investigated earlier.[14,15,23]

First, a search for possible stable conformations of **2** was done theoretically by using the CREST program[19] utilizing the GFN2-xTB method[20] for solving the electronic problem. Structures with relative energies below 3 kcal mol^{-1} were manually inspected and (symmetry) duplicates were sorted out. This resulted in seven distinct conformations, denoted here as **2a–2g** (see Figure 14).

An additional stretched conformation **2h** was also included in this set as a structure with the largest distance between the phenyl rings. The selected structures were optimized by using the CP2K program[27] and the implemented method GFN1-xTB within.[28] The relative energies and the most important torsion angles of the optimized structures are provided in Table S31

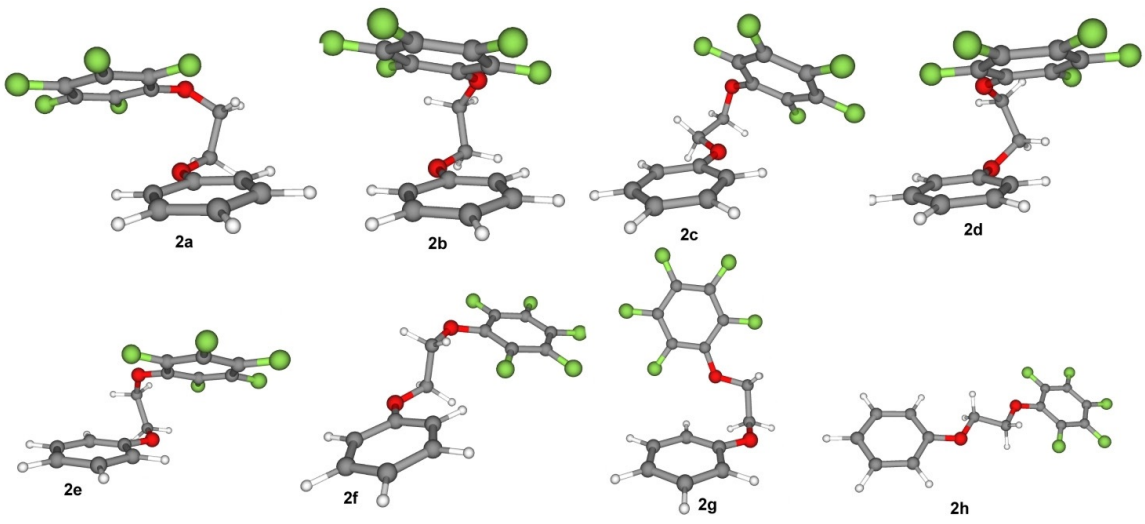

Figure 14. Selected conformers **2a–h** obtained by using the GFN1-xTB method.

(in the Supporting Information). Path integral molecular dynamics simulations were performed by using the same program and method. Eight simulations with 16 beads were performed starting from structures of each conformation. Each trajectory was 100 ps long with a step size of 0.5 fs. Distributions of the most important torsion angles (ϕ_1, θ_1, τ, θ_2, ϕ_2; see Scheme 3) were obtained from these trajectories and analyzed (see Figures S69–S73 in the Supporting Information).

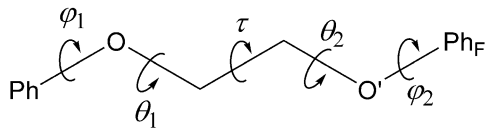

Scheme 3. Torsion angles for ethylenedioxy-bridged bisarenes **2**.

Guided by the distributions, the individual trajectories were used for calculations of interatomic vibrational amplitudes and corrections to equilibrium structures, employing the Qassandra program.[29]

For the refinement of molecular structures, a new method has been implemented into the UNEX program.[30] This method is based on the well-known regularization technique[31] and allows decoupled definition of refined structural parameters and regularization parameters of different types. For example, in this work, we defined and refined molecular structures in terms of Cartesian coordinates but the regularization was applied in terms of internal parameters, that is, bond lengths, valence, torsion, and out of plane angles. In contrast, the already available methods[32–35] apply flexible restraints only to the refined parameters. In some cases, for example, for carbaboranes,[36] it is convenient to refine and regularize Cartesian coordinates simultaneously. However, for flexible and large molecules this can either hinder the fitting of the model or can lead to highly unstable solutions. Thus, in this work, the following least-squares functional was minimized:

$$Q = \sum_i w_i \left(sM_{(i),\mathrm{exp}} - sM_{(i),\mathrm{model}}\right)^2 + \alpha \sum_j w_j \left(p_{(j),\mathrm{reg}} - p_{(j),\mathrm{model}}\right)^2 \quad (1)$$

where $sM_{(i),\mathrm{exp}}$ and $sM_{(i),\mathrm{model}}$ are experimental and model molecular intensity functions, $p_{(j),\mathrm{reg}}$ and $p_{(j),\mathrm{model}}$ are regularization and model internal geometrical parameters, w_i and w_j are respective weighting factors, α is the global regularization factor. Weighting factors for the experimental data were calculated from the corresponding individual standard deviations σ_i as $w_i = \sigma_i^{-2}$. In the regularization part of the functional, weighting factors w_j had different values depending on the location of the parameters. Relative values of w_j for valence angles in the -O-CH_2-CH_2-O- chain were smaller by a factor of 10^2 than all other valence angles. Analogously, for the torsion angles in this fragment (ϕ_1, θ_1, τ, θ_2, ϕ_2) w_j were 25 times smaller than for other torsion angles. Thus, in the refinements the inverse problem was more flexible for parameters determining conformations whereas for the benzene rings and atoms connected to them a stronger regularization was applied. To obtain regularization parameters of reasonable accuracy, the structures were additionally optimized at the PBEh-3c level of theory[37] as implemented in the Turbomole 7.4 program package.[38] The obtained torsion angles and relative energies are collected in Table S32 (in the Supporting Information). Note that functional (1) consists of two parts, (a) the first part built on experimental $sM(s)$ functions and (b) the second regularizing theoretical part. As the structures are determined by minimizing the complete functional Q, both parts of the functional can determine the refined parameters. However, the extent of influence of each part of Q on different parameters can also be different. Accordingly, contributions can be defined as a measure of influence of the parts of Q on refined parameters.

The global regularization factor α was manually adjusted so that contributions of the experimental GED data on the refined parameters were maximized while the solutions were still stable. The contributions of experimental data and regularization data, respectively, were calculated according to the W2 method.[39] Amplitudes of vibrations were refined in groups keeping the ratios within groups fixed at theoretical values. Models of all conformers were refined in exactly the same manner with the same extents of regularization. The resulting wR factors of all models and corresponding torsion angles are collected in Table 3. Note that the stated uncertainties are purely experimental errors, which were calculated by using a method removing the influence of regularization.[40] In comparison with these values, the least-squares standard deviations

Table 3. Refined torsion angles (in degrees), weighted R factors (in %), and relative energies ΔE (in kJ mol^{-1}) for all tested conformers of **2**.[a]

	ϕ_1	θ_1	τ	θ_2	ϕ_2	wR[b]	ΔE (GFN1-xTB)	ΔE (PBEh-3c)
2a	−17.8(32)	−65.9(34)	−59.8(21)	75.9(14)	72.8(22)	3.62	0.00	0.00
2b	−8.1(71)	−120.7(31)	82.1(25)	−54.3(47)	−76.4(16)	4.78	3.89	0.46
2c	14.6(59)	166.7(51)	−71.0(36)	71.6(36)	−105.0(18)	3.59	3.10	0.21
2d	−47.1(45)	−104.8(28)	58.9(19)	36.7(24)	−129.6(14)	3.60	6.44	6.02
2e	23.3(150)	70.9(43)	50.2(10)	43.0(18)	71.4(17)	5.15	7.78	9.92
2f	−20.0(300)	−80.5(130)	−179.7(25)	−78.5(88)	−57.2(20)	5.24	6.23	12.38
2g	157.3(74)	109.7(21)	−70.9(33)	145.3(25)	63.4(20)	4.14	5.69	13.05
2h	0.0	180.0	180.0	180.0	180.0	11.10	8.83	18.66

[a] In parentheses are 1σ pure experimental errors, see text for details. [b] Calculated as $wR = [\Sigma w_i\{sM_{(i),\mathrm{exp}} - sM_{(i),\mathrm{model}}\}^2 / \Sigma w_i\{sM_{(i),\mathrm{exp}}\}^2]^{1/2} \times 100\,\%$.

were unrealistically small in many cases (see Table S33 in the Supporting Information).

Other detailed information on refinements, including complete structures, is provided in the Supporting Information. The radial distribution functions are shown in Figure 15. Summarizing the results of the structural analysis of **2** by GED, we conclude that the experimental gas electron diffraction intensities are best described by the models of conformers with folded structures **2a**, **2c**, and **2d** (see Figure 16). However, it was impossible to determine exactly which of these three conformations exist in the gas phase at the experimental conditions.

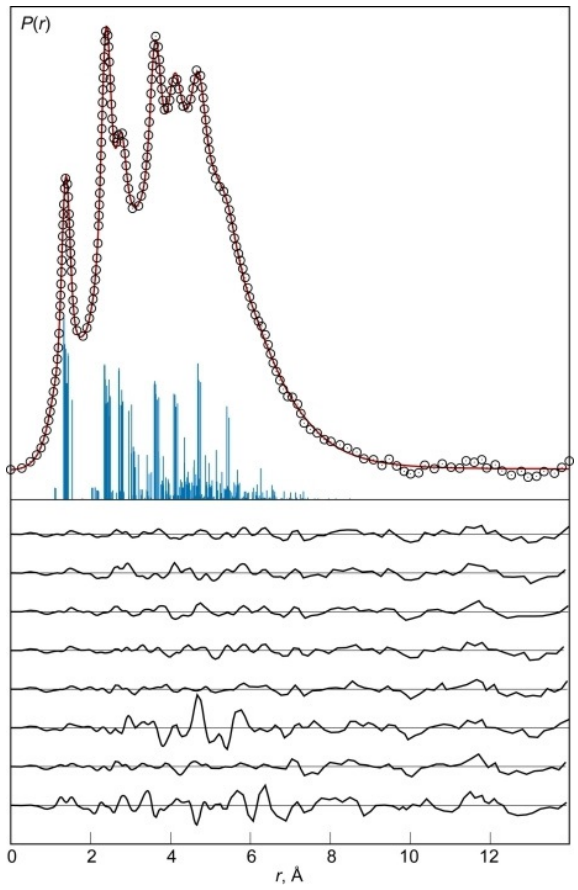

Figure 15. Experimental (dots) and best model (line) radial distribution functions of **2**. Below are the ordered difference curves for all tested models, highest for the first conformation **2a**, lowest for **2h**. Vertical bars indicate positions of interatomic distances in **2a**.

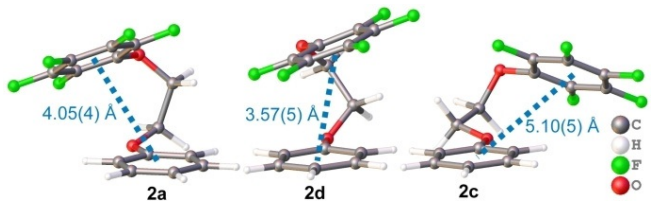

Figure 16. Conformers **2a**, **2d**, **2c** with best description of GED.

Although the models described above fit the data well, there are still small systematic differences between experimental and model radial distribution functions (Figure 15) and molecular intensity functions (Figure S68 in the Supporting Information). This was also seen by comparing the very low experimental w*R* factors of 1.6%, demonstrating the excellent reproducibility of the experimental *sM*(*s*) functions, with the best structural w*R* factors of 3.6%. It is possible that all three conformers, **2a**, **2c**, and **2d**, exist in the gas phase simultaneously.

However, a refinement of the conformational composition could not be done with sufficient accuracy by using solely the GED data owing to the instability of the inverse problem.

Interestingly, model **2b** had a somewhat larger *wR* factor in spite of its folded structure and low relative energy at the PBEh3-c level. We do not exclude that this was due to imperfections in the description of molecular vibrations on the level of molecular dynamics used in this work. For **2**, this problem is very complicated owing to the occurrence of large amplitude motions and its rich conformational landscape, which can be seen from the distributions of the torsion angles (Figures S69–S73 in the Supporting Information). In general, the stretched structures showed a worse agreement with the experimental intensities. This is also clear by comparing the difference curves of the radial distribution functions in Figure 15. The model of **2g** showed an interesting possible case of a σ–π interaction. The energy of this conformer was fairly high but the *wR* factor was relatively low. We cannot exclude small fractions of this conformer in the gas phase. The worst agreement with experimental data had model **2h** with the largest distance between phenyl rings. A special note should be made concerning the refined torsion angles in Table 3. Owing to the aforementioned vibrational complexity and ambiguity in the conformational composition, they can be significantly biased away from true equilibrium values. Moreover, in the rejected models, they do not indicate a correspondence to real structures, possibly existing in small fractions under experimental conditions.

The best GED models have folded structures with short intramolecular aryl–aryl interactions. The respective centroid–centroid distances (see Figure 16) are slightly longer than for our preliminary calculations for the gas phase (Figure 3) and comparable to GED data for bisarenes that our group investigated recently ($PhCH_2CH_2CH_2Ph_f$: 3.50(2) Å; $PhSiMe_2SiMe_2Ph_f$: 3.76(3) Å).[14,23] Note, the distances between centroids in **2** refined in this work were essentially experimental in spite of using quantum-chemically calculated restraints. W2 contributions of the GED data to these parameters are as described above and which were 97, 57, and 82% in **2a**, **2c**, and **2d**, respectively.

Conclusion

The aggregation motifs in the solid-state structures of partially fluorinated ethylenedioxy-bridged bisarenes are stabilized by intermolecular interactions. Short centroid–centroid distances to neighboring molecules in the crystal lattice are found between aromatic ring systems and fluorinated aromatics. For stronger aryl–aryl interactions, the size of the aromatic group

is important. Multiple ring systems (>Ph), support aryl contacts to more than one neighboring molecule in the crystal lattice and lead to highly ordered columnar structures. Solid-state structures of symmetric bisarenes show that the intermolecular aryl contacts are disfavored for non-halogenated aromatic systems.

The investigation of molecules by computational methods predicts the preferred formation of folded structures with intramolecular interactions for halogenated bisarenes. The oxygen atoms in the flexible ethylenedioxy backbone neither influence the polarization of the aromatic ring systems nor the conformational preference of the bisarenes significantly. Increasing the size and number of aryl interaction partners results in decreasing centroid–centroid distances and higher stabilization energies. Owing to different methods, we could prove that the stabilization of folded conformers is caused by both electrostatic attraction and dispersion interactions in the cases where two electronically different aryl groups interact with one another. For two identical groups, the electrostatic terms vanish, but a substantial stabilization by dispersion forces remains. Only in the case of the non-halogenated bisarene **7**, neither electrostatic nor dispersion is strong enough to stabilize a folded conformer.

A new method for structure refinement from the measured GED data allowed the detailed investigation of conformations for compound **2**. The obtained results confirm the hypothesis that in the gas phase for this compound folded conformations are primarily populated.

Acknowledgements

We thank Klaus-Peter Mester and Marco Wißbrock for recording NMR spectra and Barbara Teichner for elemental analyses. We also thank Timo Glodde and Dr. Jan Schwabedissen for the gas electron diffraction experiments. This work was funded by DFG (German Research Foundation) in the Priority Program SPP 1807 "Control of LD in molecular chemistry" (grant MI477/28-2, project no. 271386299) and the core facility GED@BI (grant MI477/35-1, project no. 324757882). Yu V. V. is grateful for financial support by Deutsche Forschungsgemeinschaft (DFG, Grant VI 713/1–2, project no. 243500032) and to HPC facilities at the Universität zu Köln for providing computational time and programs. Open access funding enabled and organized by Projekt DEAL.

Conflict of interest

The authors declare no conflict of interest.

Keywords: bridged arenes · dispersion interactions · gas electron diffraction · halogenated arenes · inter/intramolecular stacking interactions · solid-state structures

[1] E. A. Meyer, R. K. Castellano, F. Diederich, *Angew. Chem. Int. Ed.* **2003**, *42*, 1210 – 1250; *Angew. Chem.* **2003**, *115*, 1244 – 1287.
[2] S. K. Burley, G. A. Petsko, *Science* **1985**, *229*, 23 – 28.
[3] C. A. Hunter, *Chem. Soc. Rev.* **1994**, *23*, 101 – 109.
[4] a) E. R. T. Tiekink, J. Zukerman-Schpector, *The Importance of π-Interactions in Crystal Engineering: Frontiers in Crystal Engineering*, Wiley, Hoboken, **2012**; b) G. R. Desiraju, J. J. Vittal, A. Ramanan, *Crystal Engineering: A Textbook*, World Scientific, Singapore, **2011**; c) G. W. Coates, A. R. Dunn, L. M. Henling, J. W. Ziller, E. B. Lobkovsky, R. H. Grubbs, *J. Am. Chem. Soc.* **1998**, *120*, 3641 – 3649.
[5] E. G. Cox, D. W. J. Cruickshank, J. A. S. Smith, *Proc. R. Soc. London Ser. A* **1958**, https://doi.org/10.1098/rspa.1958.0167.
[6] J. Hernández-Trujillo, F. Colmenares, G. Cuevas, M. Costas, *Chem. Phys. Lett.* **1997**, *265*, 503 – 507.
[7] A. P. West, S. Mecozzi, D. A. Dougherty, *J. Phys. Org. Chem.* **1997**, *10*, 347 – 350.
[8] N. Boden, P. P. Davis, C. H. Stam, G. A. Wesselink, *Mol. Phys.* **1973**, *25*, 81 – 86.
[9] J. H. Williams, *Acc. Chem. Res.* **1993**, *26*, 593 – 598.
[10] C. R. Patrick, G. S. Prosser, *Nature* **1960**, *187*, 1021.
[11] a) F. London, *Z. Phys.* **1930**, *63*, 245 – 279; b) J. P. Wagner, P. R. Schreiner, *Angew. Chem. Int. Ed.* **2015**, *54*, 12274 – 12296; *Angew. Chem.* **2015**, *127*, 12446 – 12471.
[12] a) B. W. Gung, J. C. Amicangelo, *J. Org. Chem.* **2006**, *71*, 9261 – 9270; b) S. Tsuzuki, T. Uchimaru, M. Mikami, *J. Phys. Chem. A* **2006**, *110*, 2027 – 2033; c) M. O. Sinnokrot, C. D. Sherrill, *J. Am. Chem. Soc.* **2004**, *126*, 7690 – 7697.
[13] a) A. S. Shetty, J. Zhang, J. S. Moore, *J. Am. Chem. Soc.* **1996**, *118*, 1019 – 1027; b) M. L. Renak, G. P. Bartholomew, S. Wang, P. J. Ricatto, R. J. Lachicotte, G. C. Bazan, *J. Am. Chem. Soc.* **1999**, *121*, 7787 – 7799; c) F. Cozzi, F. Ponzini, R. Annunziata, M. Cinquini, J. S. Siegel, *Angew. Chem. Int. Ed. Engl.* **1995**, *34*, 1019 – 1020; *Angew. Chem.* **1995**, *107*, 1092 – 1094; d) F. Cozzi, J. S. Siegel, *Res. Prog. Chem. Phys. Biochem. Phys.* **1995**, *67*, 683 – 689.
[14] S. Blomeyer, M. Linnemannstöns, J. H. Nissen, J. Paulus, B. Neumann, H.-G. Stammler, N. W. Mitzel, *Angew. Chem. Int. Ed.* **2017**, *56*, 13259 – 13263; *Angew. Chem.* **2017**, *129*, 13443 – 13447.
[15] M. Linnemannstöns, J. Schwabedissen, B. Neumann, H.-G. Stammler, R. J. F. Berger, N. W. Mitzel, *Chem. Eur. J.* **2020**, *26*, 2169 – 2173.
[16] J. H. Williams, J. K. Cockcroft, A. N. Fitch, *Angew. Chem. Int. Ed. Engl.* **1992**, *31*, 1655 – 1657; *Angew. Chem.* **1992**, *104*, 1666 – 1669.
[17] C. R. Martinez, B. L. Iverson, *Chem. Sci.* **2012**, *3*, 2191 – 2201.
[18] T. A. Keith, AIMAll (version 19.10.12), TK Gristmill Software, Overland Park KS, USA, 2019, (aim.tkgristmill.com).
[19] a) P. Pracht, F. Bohle, S. Grimme, *Phys. Chem. Chem. Phys.* **2020**, *22*, 7169 – 7192; b) S. Grimme, *J. Chem. Theory Comput.* **2019**, *15*, 2847 – 2862.
[20] C. Bannwarth, S. Ehlert, S. Grimme, *J. Chem. Theory Comput.* **2019**, *15*, 1652 – 1671.
[21] a) A. D. Becke, *Phys. Rev. A* **1988**, *38*, 3098 – 3100; b) S. Grimme, S. Ehrlich, L. Goerigk, *J. Comput. Chem.* **2011**, *32*, 1456 – 1465.
[22] *Gaussian 16*, *Revision C.01*, M. J. Frisch, G. W. Trucks, H. B. Schlegel, G. E. Scuseria, M. A. Robb, J. R. Cheeseman, G. Scalmani, V. Barone, G. A. Petersson, H. Nakatsuji, X. Li, M. Caricato, A. V. Marenich, J. Bloino, B. G. Janesko, R. Gomperts, B. Mennucci, H. P. Hratchian, J. V. Ortiz, A. F. Izmaylov, J. L. Sonnenberg, D. Williams-Young, F. Ding, F. Lipparini, F. Egidi, J. Goings, B. Peng, A. Petrone, T. Henderson, D. Ranasinghe, V. G. Zakrzewski, J. Gao, N. Rega, G. Zheng, W. Liang, M. Hada, M. Ehara, K. Toyota, R. Fukuda, J. Hasegawa, M. Ishida, T. Nakajima, Y. Honda, O. Kitao, H. Nakai, T. Vreven, K. Throssell, J. A. Montgomery, Jr., J. E. Peralta, F. Ogliaro, M. J. Bearpark, J. J. Heyd, E. N. Brothers, K. N. Kudin, V. N. Staroverov, T. A. Keith, R. Kobayashi, J. Normand, K. Raghavachari, A. P. Rendell, J. C. Burant, S. S. Iyengar, J. Tomasi, M. Cossi, J. M. Millam, M. Klene, C. Adamo, R. Cammi, J. W. Ochterski, R. L. Martin, K. Morokuma, O. Farkas, J. B. Foresman, D. J. Fox, Gaussian, Inc., Wallingford CT, **2016**.
[23] M. Linnemannstöns, J. Schwabedissen, A. A. Schultz, B. Neumann, H.-G. Stammler, R. J. F. Berger, N. W. Mitzel, *Chem. Commun.* **2020**, *56*, 2252 – 2255.
[24] E. G. Buchanan, E. L. Sibert, T. S. Zwier, *J. Phys. Chem. A* **2013**, *117*, 2800 – 2811.
[25] X. Guo, X. Ma, Q. Yang, J. Xu, L. Huang, J. Jia, J. Shan, L. Liu, W. Chen, H. Chu, J. Wei, X. Zhang, H. Sun, Y. Tang, Q. You, *Eur. J. Med. Chem.* **2014**, *81*, 89 – 94.
[26] C. Janiak, *J. Chem. Soc. Dalton Trans.* **2000**, *21*, 3885 – 3896.

[27] H. Jürg, M. Iannuzzi, F. Schiffmann, J. Van de Vondele, *Wiley Interdiscip. Rev.: Comput. Mol. Sci.* **2014**, *4*, 15 – 25.
[28] S. Grimme, C. Bannwarth, P. Shushkov, *J. Chem. Theory Comput.* **2017**, *13*, 1989 – 2009.
[29] Y. V. Vishnevskiy, D. Tikhonov, *Theor. Chem. Acc.* **2016**, *135*, 88.
[30] Yu. V. Vishnevskiy, 2020, UNEX version 1.6, http://unexprog.org (accessed April 29 2020).
[31] A. N. Tikhonov, A. V. Goncharsky, V. V. Stepanov, A. G. Yagola, *Numerical Methods for the Solution of Ill-Posed Problems*, Springer, Dordrecht, **1995**.
[32] L. S. Bartell, D. J. Romenesko, T. C. Wong, *Molecular Structure by Diffraction Methods*, The Chemical Society, Burlington House, London, **1975**, 72 – 79.
[33] N. W. Mitzel, D. W. H. Rankin, *Dalton Trans.* **2003**, *19*, 3650 – 3662.
[34] I. V. Kochikov, Y. I. Tarasov, G. M. Kuramshina, V. P. Spiridonov, A. G. Yagola, T. G. Strand, *J. Mol. Struct.* **1998**, *445*, 243 – 258.
[35] Y. V. Vishnevskiy, M. A. Abaev, A. N. Rykov, M. E. Gurskii, P. A. Belyakov, S. Yu, Erdyakov, Y. N. Bubnov, N. W. Mitzel, *Chem. Eur. J.* **2012**, *18*, 10585 – 10594.
[36] Y. V. Vishnevskiy, D. S. Tikhonov, C. G. Reuter, N. W. Mitzel, D. Hnyk, J. Holub, D. A. Wann, P. D. Lane, R. J. F. Berger, S. A. Hayes, *Inorg. Chem.* **2015**, *54*, 11868 – 11874.
[37] S. Grimme, J. G. Brandenburg, C. Bannwarth, A. Hansen, *J. Chem. Phys.* **2015**, *143*, 054107.
[38] TURBOMOLE V7.4 2019, a Development of University of Karlsruhe and Forschungszentrum Karlsruhe GmbH, 1989 – 2007, TURBOMOLE GmbH, since 2007; http://www.turbomole.com.
[39] T. Baše, J. Holub, J. Fanfrlík, D. Hnyk, P. D. Lane, D. A. Wann, Yu. V. Vishnevskiy, D. Tikhonov, C. G. Reuter, N. W. Mitzel, *Chem. Eur. J.* **2019**, *25*, 2313 – 2321.
[40] D. S. Tikhonov, Yu. V. Vishnevskiy, A. N. Rykov, O. E. Grikina, L. S. Khaikin, *J. Mol. Struct.* **2017**, *1132*, 20 – 27.

Manuscript received: July 10, 2020
Accepted manuscript online: August 26, 2020
Version of record online: October 23, 2020